



## Data assimilation of incoherent scatter radar observation into a one-dimensional midlatitude ionospheric model by applying ensemble Kalman filter

Xinan Yue,<sup>1,2,3</sup> Weixing Wan,<sup>1</sup> Libo Liu,<sup>1</sup> Fei Zheng,<sup>3,4</sup> Jiuhou Lei,<sup>5</sup>  
Biqiang Zhao,<sup>1</sup> Guirong Xu,<sup>1,2,3</sup> Shun-Rong Zhang,<sup>6</sup> and Jiang Zhu<sup>4</sup>

Received 24 January 2007; revised 3 August 2007; accepted 21 August 2007; published 14 December 2007.

[1] In this paper, electron densities during 25–28 September 2000 observed by the Millstone Hill incoherent scatter radar (ISR) are assimilated into a one-dimensional midlatitude ionospheric theoretical model by using an ensemble Kalman filter (EnKF) technique. It is found that (1) the derived vertical correlation coefficients of electron density show obvious altitude dependence. These variations are consistent with those from ISR observations. (2) The EnKF technique has a better performance than the 3DVAR technique especially in the data-gap regions, which indicates that the EnKF technique can extend the influences of observations from data-rich regions to data-gap regions more effectively. (3) Both the altitude and local time variations of the root mean square error (RMSE) of electron densities for the ensemble spread and ensemble mean from observation behave similarly. It is shown that the spread of the ensemble members can represent the deviations of ensemble mean from observations. (4) To achieve a better prediction performance, the external driving forces should also be adjusted simultaneously to the real weather conditions. For example, the performance of prediction can be improved by adjusting neutral meridional wind using equivalent wind method. (5) In the EnKF, there are often erroneous correlations over large distance because of the sampling error. This problem may be avoided by using a relative larger ensemble size.

**Citation:** Yue, X., W. Wan, L. Liu, F. Zheng, J. Lei, B. Zhao, G. Xu, S.-R. Zhang, and J. Zhu (2007), Data assimilation of incoherent scatter radar observation into a one-dimensional midlatitude ionospheric model by applying ensemble Kalman filter, *Radio Sci.*, 42, RS6006, doi:10.1029/2007RS003631.

### 1. Introduction

[2] It is now well known that the ionosphere displays both a background state (climatology) and a disturbed state (weather) [Rishbeth and Mendillo, 2001]. The ionospheric climatology has been successfully represented by

both empirical and theoretical models developed in the past [e.g., Anderson, 1973a, 1973b; Bilitza, 2001; Bailey *et al.*, 1997; Fuller-Rowell *et al.*, 2002; Huba *et al.*, 2000; Richards and Torr, 1985; Roble *et al.*, 1988; Schunk *et al.*, 1998; Sojka and Schunk, 1985]. However, it has been much more difficult to model the ionospheric weather with both types of models because empirical models are statistically constructed based on observations, whereas the accuracy of theoretical models often depends on the accuracy of external drivers. The ionospheric weather can have detrimental effects on several human activities and operational systems, including high-frequency communications, over-the-horizon radars, and survey and navigation systems using Global Positioning System (GPS) satellites. To avoid the destructive effects of ionospheric weather on military and civilian systems, there is a growing need to more accurately represent and forecast the ionosphere. Recently, many groups attempt to incorporate observations into ionospheric models by using optimization schemes, which are known as data

<sup>1</sup>Institute of Geology and Geophysics, Chinese Academy of Sciences, Beijing, China.

<sup>2</sup>Wuhan Institute of Physics and Mathematics, Chinese Academy of Sciences, Wuhan, China.

<sup>3</sup>Graduate School, Chinese Academy of Sciences, Beijing, China.

<sup>4</sup>Institute of Atmospheric Physics, Chinese Academy of Sciences, Beijing, China.

<sup>5</sup>High Altitude Observatory, National Center for Atmospheric Research, Boulder, Colorado, USA.

<sup>6</sup>Haystack Observatory, Massachusetts Institute of Technology, Westford, Massachusetts, USA.

assimilation methods, to give specific representation of ionosphere [Hajj et al., 2000, 2004; Pi et al., 2003, 2004a, 2004b; Schunk et al., 2003, 2004, 2005; Wang et al., 2004; Scherliess et al., 2004, 2006a, 2006b; Mandrake et al., 2005; Thompson et al., 2006]. Data assimilation methods incorporate continuous observations into models, providing a global/regional description of a system that is optimally consistent with both model and data. These methods have been highly successful in weather and climate modeling in meteorology and oceanography, and form the basis of Numerical Weather Prediction (NWP) models routinely used for weather forecastings. The standard data assimilation cycle consists of quality control (to check the validity of the observations), objective analysis (to generate a complete analysis field with the model results and observations), and forecast (to propagate the state forward in time) [Bust et al., 2004; Daley, 1991]. Several necessary components to build a data assimilation model include a forward model (which can propagate the state forward in time), observations (which will be mapped to the model state by an observation operator), and an optimization method (which can give an optimal analysis by ingesting observations into the model) [see Daley, 1991; Pi et al., 2003]. Various optimization methods, such as optimal interpolation, variational methods (include three-dimensional and four-dimensional variation), and Kalman filter (KF), have been widely used by meteorologists and oceanographers for several decades and encouraging achievements have been obtained [Bouttier and Courtier, 1999]. A more detailed description of the terminology and methods can be found in the works of Bouttier and Courtier [1999], Daley [1991], Kalnay [2003], Maybeck [1979], and Talagrand [1997]. With the significant increase in ionospheric observations and the speed of the computers, data assimilation also became a powerful technique, providing a better specification and forecasting of the global ionosphere [Schunk et al., 2004; Wang et al., 2004].

[3] There is a growing interest in assimilating empirical models [Angling and Cannon, 2004; Bust et al., 2004; Howe et al., 1998; Schlüter et al., 2003; Spencer et al., 2004; Stolle et al., 2006]. The major limitation of data assimilation based on empirical model is lack of prediction capability because they do not deal with the physical processes and so can not propagate the state forward in time. There are many techniques that can be used to propagate the state forward including using Gauss-Markov Kalman filter and using a physics based model. The Gauss-Markov process assumes that the errors of the state grow at an exponential rate with time, allowing the state to relax back to climatology according to a specific timescale if observations have become unavailable [Fuller-Rowell et al., 2004; Scherliess et al., 2006a, 2006b]. A physical based model can advance

the state from one time to the next on the basis of several dynamical equations and external drivers. Assimilative models that use first-principles physical models attempt to merge the benefits of observations and physical models and provide an improved forecasting. These ionospheric data assimilation models include the University of Southern California/the Jet Propulsion Laboratory Global Assimilative Ionospheric Model (USC/JPL GAIM) [Hajj et al., 2000, 2004; Mandrake et al., 2005; Pi et al., 2003, 2004a, 2004b; Wang et al., 2004], the Utah State University Global Assimilation of Ionospheric Measurements (USU GAIM) [Scherliess et al., 2004, 2006a, 2006b; Schunk et al., 2003, 2004, 2005; Thompson et al., 2006], and the IonoNumerics model [Khattatov et al., 2004, 2005]. At the same time, the observations including electron densities, plasma drifts, magnetometer measurements, and so on are also assimilated into models to accomplish some scientific researches [Eccles, 2004; Lei et al., 2004b, 2004c; Retterer et al., 2005; Richmond and Kamide, 1988; Richmond et al., 1988; Sojka et al., 2001, 2003; Zhang et al., 1999, 2001, 2002, 2003]. In the ionospheric data assimilation applications, a majority of the employed data assimilation methods are 3DVAR [Bust et al., 2004], 4DVAR [Pi et al., 2003, 2004a, 2004b], and Kalman filter or its approximations [Fuller-Rowell et al., 2004; Hajj et al., 2004; Scherliess et al., 2004]. In comparison with 3DVAR, Kalman filter can propagate the background error covariance forward dynamically and this is its primary reason why many researchers prefer it to other methods [Kalnay, 2003]. Kalman filter is proved to be equivalence to 4DVAR, except that Kalman filter externally forwards the error covariance while 4DVAR internally; Kalman filter does not need an adjoint, and 4DVAR relies on the hypothesis that the model is perfect [Bouttier and Courtier, 1999]. Therefore Kalman filter has been more widely used in ionospheric data assimilation investigations than other methods. However, the Kalman filter takes an assumption that the model should be linear which most ionospheric models do not satisfy [Scherliess et al., 2004]. Though the extended Kalman filter has been developed to overcome this issue, it can only make a suboptimal estimation and may result in filtering divergence problem when the system is highly nonlinear [Welch and Bishop, 2004]. If we want to use Kalman filter in a nonlinear system, the model should be linearized. This is not practical for a highly nonlinear system. Furthermore, full implementation of the Kalman filter is not practical for large dimensional problems, and therefore many approximations such as band-limited Kalman filter or reduced-state approximation are usually used [Hajj et al., 2004; Scherliess et al., 2004].

[4] To overcome the difficulties that Kalman filter has been confronted with, many meteorologists and oceanographers attempted to introduce Monte Carlo based

methods to approximate Kalman filter (EnKF) [Anderson and Anderson, 1998; Evensen, 1994, 2003; Evensen and van Leeuwen, 1996; Houtekamer and Mitchell, 1998, 2001; Mitchell and Houtekamer, 2000; Mitchell et al., 2002]. In the EnKF, the error statistics are calculated from an ensemble of the forward model forecasts which run in parallel. The EnKF was first introduced by Evensen [1994] and has become popular recently because of its simple conceptual formulation and relative ease of implementation. It requires neither derivation of a tangent linear operator or adjoint equations nor integrations backward in time [Evensen, 2003]. The EnKF has been widely examined and applied in meteorology and oceanography in the past decade. In this paper, we will explore the feasibility of assimilating incoherent scatter radar (ISR) observations into a theoretical ionospheric model by this method. To validate this method, we will also compare the assimilated results between 3DVAR and EnKF.

[5] Although there are many outstanding ionospheric data assimilation models, it is of great importance for us to continue the investigation about ionospheric data assimilation for methodical, practical, and scientific reasons as follows. (1) Every data assimilation method, such as 3DVAR, 4DVAR, KF, or EnKF, has its own advantage and shortcoming. To give a better performance of ionospheric data assimilation model, we should investigate the adaptability of different methods. EnKF, as a recent data assimilation method, has only been investigated in ionospheric or thermospheric data assimilation by few researchers [Codrescu et al., 2004; Scherliess et al., 2006a, 2006b]. So it is significant for us to implement EnKF in ionospheric assimilation for a methodological reason. In this investigation, questions associated with the influence of ensemble size on the assimilation results, and the representation of model errors, will be studied and discussed in detail. (2) The ionospheric observations are usually distributed asymmetrically in space. To provide a specific nowcasting of the ionosphere, it is important for the assimilation model to extend the influences of observations from data-rich regions to data-sparse regions. This task is usually carried out by background error covariance. Usually, 3DVAR method background error covariance and initial forecast error covariance of Kalman filter are obtained by an empirical correlation model [Bust et al., 2004]. However, the correlation coefficients of ionosphere may have temporal and spatial variations. In this investigation, we will give the altitude and local time variations of the correlation coefficients of electron densities derived from the sample covariance. The ISR observations are used to confirm its reliability. (3) As we know, the initial conditions in the theoretical model are not as so important as the model drivers because of the short time constants for electron density changes in E and F

regions [Scherliess et al., 2004]. To achieve a better prediction performance, the external driving forces should also be adjusted simultaneously under the real weather conditions [Pi et al., 2003, 2004b; Schunk et al., 2004]. In this investigation, we will improve the prediction ability of the assimilation model by using the equivalent wind method [Liu et al., 2003, 2004].

[6] The theoretical model and the observations used are presented in section 2. In section 3 we give a brief description about the assimilation methods including 3DVAR, KF, and EnKF and the representations of model and observation error. The comparisons between 3DVAR and EnKF are given in section 4. In section 5, we present the assimilated results by EnKF. Finally, discussions and conclusions are given in sections 6 and 7.

## 2. Model and Data Descriptions

[7] A one-dimensional theoretical model for the mid-latitude ionosphere [Lei et al., 2004a, 2004b; Lei, 2005] is used in this study. This model solves the equations of continuity, motion, and energy of plasma in Cartesian coordinates. In midlatitude, we can ignore the horizontal gradients of the ionosphere and so all equations are solved along the vertical direction. The default altitude range of the model is 100–600 km with the space interval of 2 km. So there are 251 points of model state between 100 and 600 km. The model time step is 18 minutes in this study. The continuity equation of the  $i$ th ion is:

$$\frac{\partial N_i}{\partial t} = P_i - \beta_i N_i - N_i \frac{\partial V_{iz}}{\partial z} - V_{iz} \frac{\partial N_i}{\partial z} \quad (1)$$

where  $P_i$  and  $\beta_i$  are production and loss rates of ion, respectively. Production rates include photoionization rates and chemical reaction production rates.  $V_{iz}$ , the vertical velocity of ions, can be calculated by combining the motion equations of electron and ions:

$$0 = -k\nabla(N_e T_e) - N_e e(\vec{E} + \vec{V}_e \times \vec{B}) \quad (2)$$

$$0 = -\kappa\nabla N_i T_i + N_i m_i \vec{g} + N_i e(\vec{E} + \vec{V} \times \vec{B}) - N_i m_i \sum_{j \neq i} v_{ij}(\vec{V}_i - \vec{V}_j) \quad (3)$$

where  $k$  is Boltzmann constant and  $V_{ij}$  is the collision frequency between  $i$ th ion and  $j$  (ion or neutral). In electron motion equation, several components related with the mass of electron are ignored. In this model, one major ion ( $O^+$ ) and three minor ions ( $O_2^+$ ,  $NO^+$ , and  $N_2^+$ ) are considered. Electron number density is assumed to be equal to the sum of all ions. Densities of minor ions are obtained under the assumption of photochemical equilibrium. The continuity equation of  $O^+$  is solved by finite

difference method with given boundaries. The assumption of photochemical equilibrium is also used in the lower boundary for  $O^+$  and model results (such as IRI) or observations can be given in the upper boundary. In this paper, observed electron density is used as upper boundary of  $O^+$ . The considered 19 chemical reactions for  $O^+(^4S)$ ,  $O^+(^2D)$ ,  $O^+(^2P)$ ,  $O_2^+$ ,  $N_2^+$ , and  $NO^+$  and corresponding reaction rates can be found in *Lei et al.* [2004a, 2004b]. The solar flux EUVAC model is used to provide EUV flux [*Richards et al.*, 1994]. Neutral gas compositions and temperature are calculated from MSIS model while neutral winds from HWM model [*Hedin*, 1991; *Hedin et al.*, 1996]. The absorption and ionization cross-sections are taken from *Richards et al.* [1994] except that the nighttime photoionization cross-sections are from *Huba et al.* [2000]. The secondary ionization is also considered according to the work of *Titheridge* [1996]. The nighttime EUV fluxes from *Strobel et al.* [1974] are used. The effects of vibrationally excited  $N_2$  and  $O_2$  on the loss rate of  $O^+$  are also considered according to *Pavlov et al.* [1999, and references therein].

[8] The energy equations for electron and  $O^+$  have been solved to obtain plasma temperatures using a similar finite difference technique as that in solving the continuity equation [*Lei*, 2005]. The temperature of  $O_2^+$ ,  $N_2^+$ , and  $NO^+$  are assumed to be equal to that of  $O^+$ . Neglecting the effects of field aligned currents, the energy equation of  $O^+$  can be represented as:

$$\frac{3}{2}N_i\kappa\frac{\partial T_i}{\partial t} = -N_i\kappa T_i\nabla\cdot\vec{V}_i - \frac{3}{2}N_i\kappa T_i\vec{V}_i\cdot\nabla T_i + \nabla\cdot(\lambda\nabla T_i) + Q \quad (4)$$

where  $i$  represents electron or  $O^+$ ,  $k$  is Boltzmann constant,  $\lambda$  is thermal conductivity, and  $V_i$  is the corresponding ion velocity. Four items on the right side of equation (4) are the heating rates due to the adiabatic compression heating, thermal diffusion, thermal conductivity, and collision interactions with other ion or neutral species, respectively. Since thermal conduction occurs primarily along the flux-tube, according to *Stubbe* [1972], the energy equation can be written as follows in midlatitude region.

$$\frac{3}{2}N_i\kappa\frac{\partial T_i}{\partial t} = \lambda\sin^2 I\frac{\partial^2 T_i}{\partial z^2} + \left(\sin^2 I\frac{\partial\lambda}{\partial z} - \frac{3}{2}N_i\kappa V_z\right)\frac{\partial T_i}{\partial z} + \kappa T_i\left(\frac{\partial N_i}{\partial t} + V_z\frac{\partial N_i}{\partial z}\right) + Q \quad (5)$$

where  $V_z$  is the vertical velocity of  $O^+$ . The heating source for electrons includes photoelectron heating, elastic collision with neutral particles ( $N_2$ ,  $O_2$  and  $O$ ), vibrational and rotational excitation of  $N_2$  and  $O_2$ , excitation of the fine structure levels of atomic oxygen, excitation from  $^3P$  to  $^1D$  state for atomic oxygen, and the

energy transfer by electron-ion collisions; for  $O^+$ , ion-electron collisions, ion-ion collisions and elastic and non-elastic collisions with the neutrals are considered [*Millward et al.*, 1996; *Schunk and Nagy*, 1978]. For the lower boundary, ion temperature equals neutral temperature, while electron temperature is obtained under the heat equilibrium assumption. Ion and electron temperatures in the upper boundary are set to be the observed values. Initial conditions of plasma densities and temperatures are given by IRI model.

[9] The Millstone Hill ISR experiment was performed from 1258 UT on 25 September 2000 to 2355 UT on 28 September 2000. The solar and geomagnetic activities during this interval are plotted in Figure 1. The maximum of Kp index is 5 and the minimum of Dst is  $-43$ . It can be concluded from the figure that there are two minor storms during this interval. The Ne, Te, and Ti altitude profiles observed by the ISR zenith antenna are used in this study. Ne profiles are fitted by the two-layer Chapman function [*Lei et al.*, 2004d]. Then we calculated the electron densities in the grid point of the model. Te and Ti in the altitude of 600 km are obtained by interpolation to be used as the upper boundaries of the model. The parameters foF2 and hmF2 are also obtained from the fitted Ne profiles. Only observed electron density between 200 and 450 km are assimilated into the model. The observations are interpolated in time direction to have a time resolution of 18 minutes, which is the same as that of our model. Both modeled and observed electron densities have resolutions of 2 km in altitude and 18 minutes in time. So the size of state and observation vectors are 251 (100–600 km) and 126 (200–450 km), respectively.

### 3. Data Assimilation Methods Descriptions and the Representations of Model and Measurement Errors

#### 3.1. 3DVAR Method

[10] In this investigation, EnKF is the primary data assimilation method. To validate this method, we also give some general comparisons with 3DVAR. The 3DVAR technique offers several features that make it useful for ionospheric specification. For example, it can easily be used in the condition that both the model and the observation operators are nonlinear; it can incorporate multiple types of data. We can obtain more specific presentations about these aspects in *Bust et al.* [2004]. The 3DVAR method is a statistical minimization method that seeks to minimize a cost function of data perturbations weighted by the observation error covariance and the derivations of the model from the background weighted by background error covariance [*Daley*, 1991]. The solution is obtained by performing several

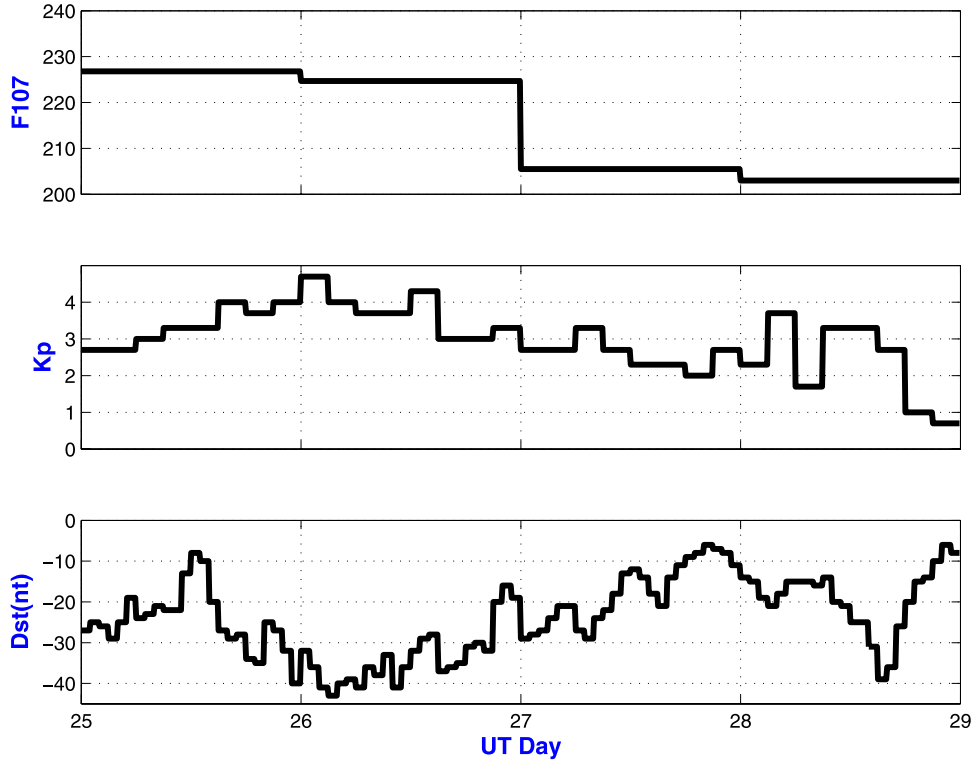


**Figure 1.** Solar and geomagnetic activities during the interval of 25–28 September 2000. We use daily F107 to represent solar activity and 3 hour Kp and 1 hour Dst to represent geomagnetic activity here.

evaluations of the cost function and of its gradient in order to approach the minimum using a suitable descent algorithm [Bouttier and Courtier, 1999]. The cost function and its gradient are represented as follows:

$$J(x) = (x - x_b)^T P^{-1} (x - x_b) + (y - H(x))^T R^{-1} (y - H(x)) \quad (6)$$

$$\nabla J(x) = 2P^{-1}(x - x_b) - 2H^T R^{-1}(y - H(x)) \quad (7)$$

where  $x$ ,  $x_b$ ,  $P$ ,  $y$ ,  $H$ , and  $R$  are the true state, background state, background error covariance, observation, observation operator, and observation error covariance respectively. Usually, the background error and observation error are assumed unbiased. The background error covariance and observation error covariance are:

$$P = e_b e_b^T, e_b = x_b - x \quad (8)$$

$$R = e_o e_o^T, e_o = y - H(x) \quad (9)$$

where  $e_b$  and  $e_o$  are background error and observation error, respectively. In this investigation, we solve the equations (6) and (7) in data space as used by Bust *et al.* [2004]. The solution of electron density  $x$  is given by

$$x = x_b + PH^T [R + HPH^T]^{-1} (y - Hx_b) \quad (10)$$

[11] In the 3DVAR data assimilation of this investigation, the one-dimensional midlatitude ionospheric model described above is used to advance the analysis from one time step to the next. The observation error and the background error are assumed to be proportional to the squares of the observation and background, respectively, as several researchers did [Angling and Cannon, 2004; Mandrake *et al.*, 2005]. The observation error is set to be independent and background error is considered to be Gaussian correlated with a fixed correlation length in the range of 100–600 km (we also can use an empirical model of correlation length which varies with altitude and local time) [Bust *et al.*, 2004]. The vertical error correlation lengths of ionospheric weather are not well known. According to Bust *et al.* [2004], the correlation length varies from 20–25 km in E and F regions to

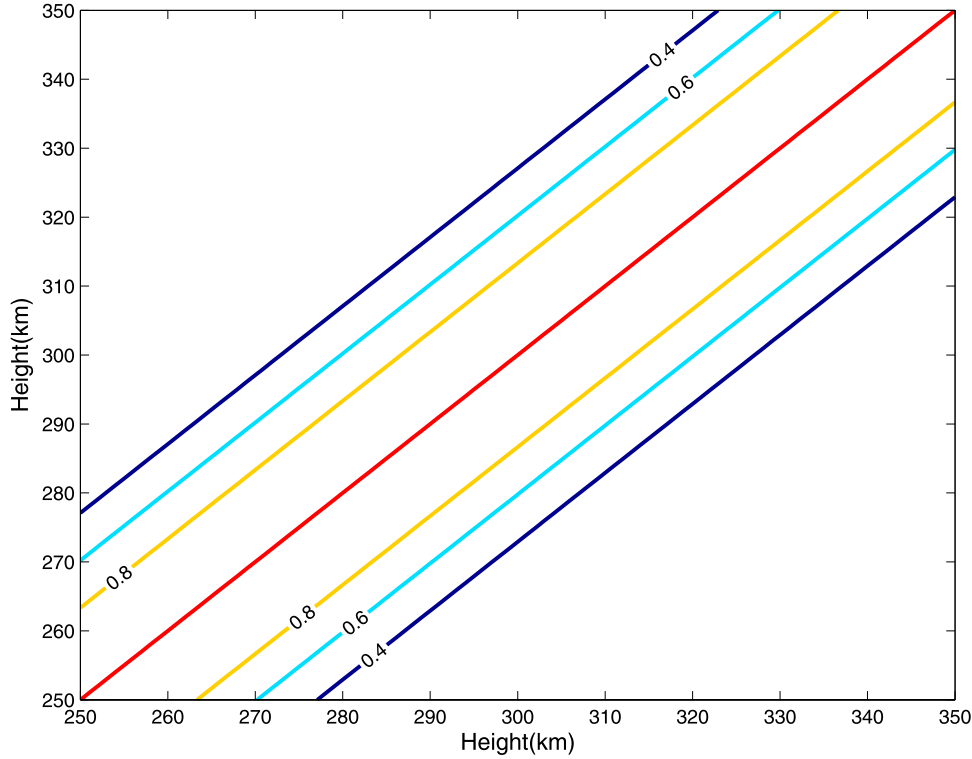


**Figure 2.** Background error correlation coefficients of electron density used in 3DVAR data assimilation between 250 and 350 km.

500 km to the plasmasphere. The correlation length of background error is assumed to be about 28 km in the 3DVAR of this paper. In this study, the background error correlation coefficients used in 3DVAR data assimilation between 250 and 350 km are shown in Figure 2. The observation and background error covariance between grid  $i$  and  $j$  are represented as follows:

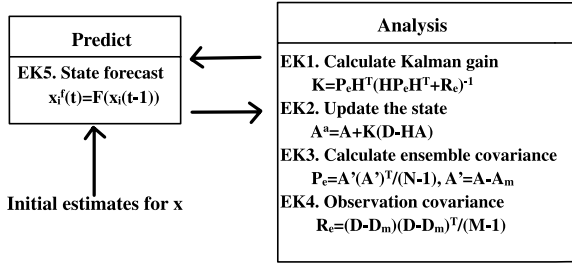
$$R_{ij} = \begin{cases} 0.043 \times N_e^i \times N_e^j, & i = j \\ 0, & i \neq j \end{cases} \quad (11)$$

$$P_{ij} = 0.43 \times N_e^i \times N_e^j \times e^{-L_{ij}^2/800} \quad (12)$$

The derivation of ratio 0.043 will be given in section 3.4. We chose the ratio of model error is 0.43. A more accurate ratio of model errors may be obtained by statistical analysis on the model results by input different model drivers including neutral information, solar and geomagnetic activities [Scherliess *et al.*, 2006a, 2006b; Thompson *et al.*, 2006].

### 3.2. EnKF Method

[12] The EnKF is based on the theory of stochastic dynamical prediction that describes the evolution of error statistics [Welch and Bishop, 2004]. It consists of a set (or ensemble) of parallel short-term forecasts and data assimilation cycles. This ensemble intends to provide a probabilistic forecast in the short term rather than at the medium range. Since, in the short term, forecast errors retain memory of the initial (analysis) errors, the EnKF must therefore incorporate probabilistic information on analysis errors in the generation of the ensemble. This is accomplished, at least approximately, by providing a set of ‘perturbed’ observations to each of the member assimilation cycles. These perturbed observations consist of actual observations plus distinct realizations of random noise, whose statistics are consistent with the assumed observational error covariance. The EnKF is related to the classic Kalman filter, which provides the optimal analysis in the case that the forecast dynamics are linear and both background and observation errors have normal distributions. The primary difference is that



where  $N$  is the number of ensemble members,  $n$  is the size of model state, and  $M$  is the number of measurements.

$A = (x_1, x_2, \dots, x_N)$ ,  $x_i$  is the ensembles members

$A_m$  is the ensemble mean

$D = (d_1, d_2, \dots, d_N)$ ,  $d_j = d + f_j$ ,  $j = 1, \dots, N$ ,  $d_j$  is the observation with perturbations and  $f$  is the observation perturbations.

$D_m$  is measurements vector.

**Figure 3.** A schematic description of the ensemble Kalman filter [from Evensen, 2003].

the KF explicitly forecasts the evolution of the complete error covariance matrix using linear dynamics, while the EnKF estimates this matrix from a sample ensemble of fully nonlinear forecasts. The EnKF also addresses the computational difficulty of propagating or even storing the forecast error covariance matrix, whose elements equal in number the square of the dimension of the forecast model (number of grid point multiplying number of variables). Under assumptions of linearity of error growth and normality of observation and forecast errors, this scheme produces the actual background error covariance as the ensemble size increases. For smaller ensembles, however, the EnKF is rank deficient and its background covariance estimates suffer from a variety of sampling errors, including spurious correlations between widely separated locations. EnKF assimilation algorithm may be able to provide a more accurate analysis under highly nonlinear and non-normal situations [Evensen, 2003]. If these assimilations algorithms can work accurately with fewer ensemble members than elements in the state vector, they will be computationally much less expensive as well. In comparison with Gauss-Markov Kalman filter based on an empirical electron density profile, the model transition error covariance of EnKF is obtained by statistical analysis on ensemble model results. The spatial and temporal evolutions of background error may be more accurate. However, its validity depends on the given uncertainties associated with model, model drivers, etc. Gauss-Markov Kalman filter may be also a good choice when the parameter such as time constant is accurately given [Fuller-Rowell et al., 2004; Howe et al., 1998; Schunk et al., 2004]. Another potential advantage of EnKF is that we may obtain an updated state of one variable (e.g. electron temperature) by

assimilating another different variable (e.g. electron density) theoretically because we can obtain the covariance between them from the ensemble state [Evensen, 2003]. A formulary description of EnKF is given in Figure 3.

[13] The ensemble number is chosen to be 10 in this paper for calculation convenient in personal computer. The implementations of EnKF are as follows. (1). At first, an ensemble of initial conditions including initial plasma densities and temperatures, initial neutral densities, temperatures, and winds, and boundary conditions (electron density and electron and ion temperatures at 600 km) of the model are obtained by adding an ensemble of stochastic normal perturbations to the corresponding variable, with ensemble mean equal to zero and variance is proportional to the square of the variable [Angling and Cannon, 2004; Evensen, 2003]. Assume  $x$  is a variable such as initial electron density at an altitude which will be perturbed, the ensemble of  $x$ ,  $X$  is obtained like this:

$$X = x + \varepsilon, \bar{\varepsilon} = 0, \sigma(\varepsilon) = r \times x^2 \quad (13)$$

where  $\sigma$  is the variance of  $\varepsilon$ . In this paper,  $\varepsilon$  is a vector of 10 elements. The values of  $r$  are chosen as follows: 10 percent for plasma and neutral densities, 5 percent for plasma and neutral temperature, and 1 percent for neutral wind and boundary conditions. These ratios are obtained by repeating running of the model with different combined values. Then we compare this different background error covariance before the analysis. When we chose the above combination, the background covariance before analysis has approximately the same ratio proportional to the square of the model results. For the observations, 10 different observation profiles are obtained by the same perturbation method as equation (13) and  $r$  is 0.043 as used in 3DVAR. The observation covariance is calculated by equation EK4 in Figure 3. (2). Then the 10 models with different initial and boundary conditions run forward in time. When there are observations which will be assimilated, background error covariance is calculated by equation EK3 in Figure 3. By using background and observation covariance, we update the ensemble model states by equation EK2. The output model results are obtained by averaging the ensemble model results. (3). Before running the 10 models forward with updated states as initial conditions, the model uncertainties should be carefully considered. The representation method of model errors is given in section 3.3. Then, we perturb the observed electron density, temperature, and ion temperature at 600 kn altitude by equation (13) with  $r$  equal to 0.01. The 10 models then run forward in time and repeat. Figure 4 illustrates a sketch map of the EnKF implementation in our investigation.

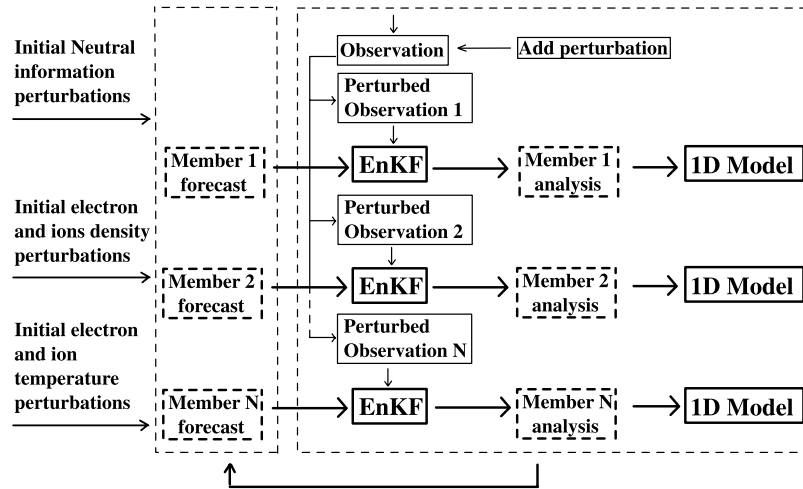


**Figure 4.** The EnKF data assimilation scheme we used.

### 3.3. Representations of Model Errors

[14] The Kalman filter includes an explicit description of the evolution of the forecast-error covariances in a data assimilation cycle. Given exact knowledge of all sources of error, linear dynamics, and a number of other conditions [Maybeck, 1979], the filter constitutes an optimal data assimilation scheme. Unfortunately, this will not be the case if there are inaccuracies in the statistical description of the error sources. Here, for instance, one may think of inaccurate model-error covariances or observational-error covariances. If the inaccuracies are too large, one may observe filter divergence [Mitchell and Houtekamer, 2000]. The EnKF data assimilation algorithm avoids the computationally expensive explicit integration of the error covariance matrix equation. Instead, the error statistics are calculated from an ensemble of short range forecasts. In EnKF assimilation method, the accuracy of error covariance is very important. Inaccurate specification of background error covariance would result in inaccurate analysis error covariance, which is then propagated forward in time. If the analysis errors are underestimated in one cycle, the forecast errors may be underestimated in the following cycle, underweighting the new observations. The process can feed back on itself, the ensemble assimilation method progressively ignoring observation more and more in successive cycles, results in filter divergence problem [Hamill, 2004].

[15] Several methods have been proposed to improve the description of model errors. Hamill [2004] has given a general review on the methods that have been developed and applied. In ionospheric data assimilation, the USU GAIM performed 1107 individual 2-day runs of the IFM with varying external forcing parameters to model

the model error [Scherliess *et al.*, 2006a, 2006b; Thompson *et al.*, 2006]. In the case of our model, the external ionospheric drivers including neutral compositions, neutral temperatures, neutral winds, solar EUV flux are all obtained by empirical models not by observations. The uncertainties associated with the use of these empirical models may result in the uncertainties of the model. In addition, the assumption of the model that there is no horizontal gradient in midlatitude, incomplete considerations of physical processes and the numerical calculations can also bring errors. In our investigation, we follow a simple method called covariance inflation [Anderson and Anderson, 1998] to modify the background error covariance. This method can simply be given:

$$X \rightarrow r(X - \bar{X}) + \bar{X} \quad (14)$$

where  $X$  represents the ensemble of the model results,  $\bar{X}$  is the ensemble mean of  $X$ . For example, if we will represent the model uncertainty of electron density at 300 km altitude.  $X$  means the 10 values of the electron density by 10 models.  $\bar{X}$  is the mean value of these 10 elements.  $\rightarrow$  means a replacement of the previous values of  $X$ ,  $r$  is the inflation factor. In this investigation,  $r$  is chosen to be equal to 1.01. Note that inflation increases the spread of the ensemble, but it does not change the subspace spanned by the ensemble. Usually the inflation factor is chosen to be slightly larger than 1. Obviously, if  $r$  is too large, the observations are given too much weight. Actually, the inflation factor should be chosen very carefully and for different model it may have different values. We have tried several values of  $r$ . By our test, when 1.01 is chosen, the time variations of ensemble spread and the deviation of ensemble mean from observations have approximately the same shape as

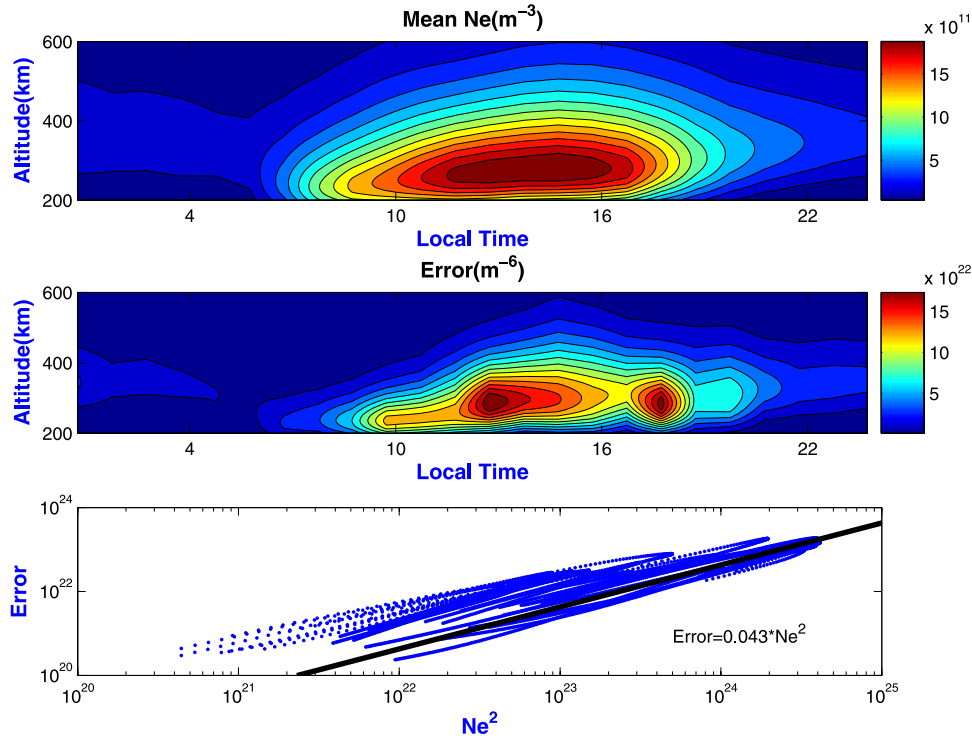


**Figure 5.** Local time and altitude variations of statistical mean electron densities and errors of electron densities obtained on ISR 27 days observations are plotted in the top and middle panels, respectively. The errors are plotted against the square of the corresponding mean electron densities for all the altitudes and local times in the lower panel, and the line is the fitted results in the form:  $y = a \cdot x$ . The fitted coefficient is also shown in the figure.

shown in Figure 8. Too small or big  $r$  will result in filter divergence. Further studies about inflation factor should be performed to obtain a best value in ionospheric data assimilation. On the other hand, other methods to represent the model errors, such as adding noise into the ensemble of forecasts and parameterized model error [Mitchell and Houtekamer, 2000], would also be explored in the further investigations.

### 3.4. Representations of Measurement Errors

[16] In both 3DVAR and EnKF method, accurately representation of measurement error is very important. It determines the weight of the observation in the assimilation results. In our investigation, the derivation of observation error is obtained by statistical analysis on the ISR observed electron densities. The observations used here are the first long-duration incoherent scatter radar (ISR) observations over Millstone Hill from 4 October to 4 November 2002. The electron density profiles were checked carefully and fitted as described in section 2. We then calculated electron densities between 200 and 600 km with 2 km interval and interpolated in time direction with one hour interval.

The data of three most disturbed days are thrown off. 24 electron density profiles of integral 27 day were obtained at last. For every hour we can calculate the error covariance matrix  $R_{201 \times 201}$  of electron profile based on statistical analysis of 27 samples. The element of error covariance is defined:

$$R_{ij} = r_{ij} \times \sigma_i \times \sigma_j \quad (15)$$

where  $r_{ij}$  is the correlation coefficient between point  $i$  and  $j$ ,  $\sigma_i$  is the standard deviation in point  $i$ . We can calculate the variance and correlation coefficient between arbitrary two points based on the obtained covariance matrix and equation (15). The correlation coefficients will be used in the discussion section.

[17] The local time and altitude variations of averaged electron densities and the variances of 27 day observations are plotted in Figure 5. According to the figure, both the altitude and local time variations of the observation variances are approximately consistent with that of mean electron densities. The variances have obvious enhancement near the sunset time. This may be due the plasma instabilities associated with the pre-reversal enhancement of EXB drift near sunset. Many researchers assumed that

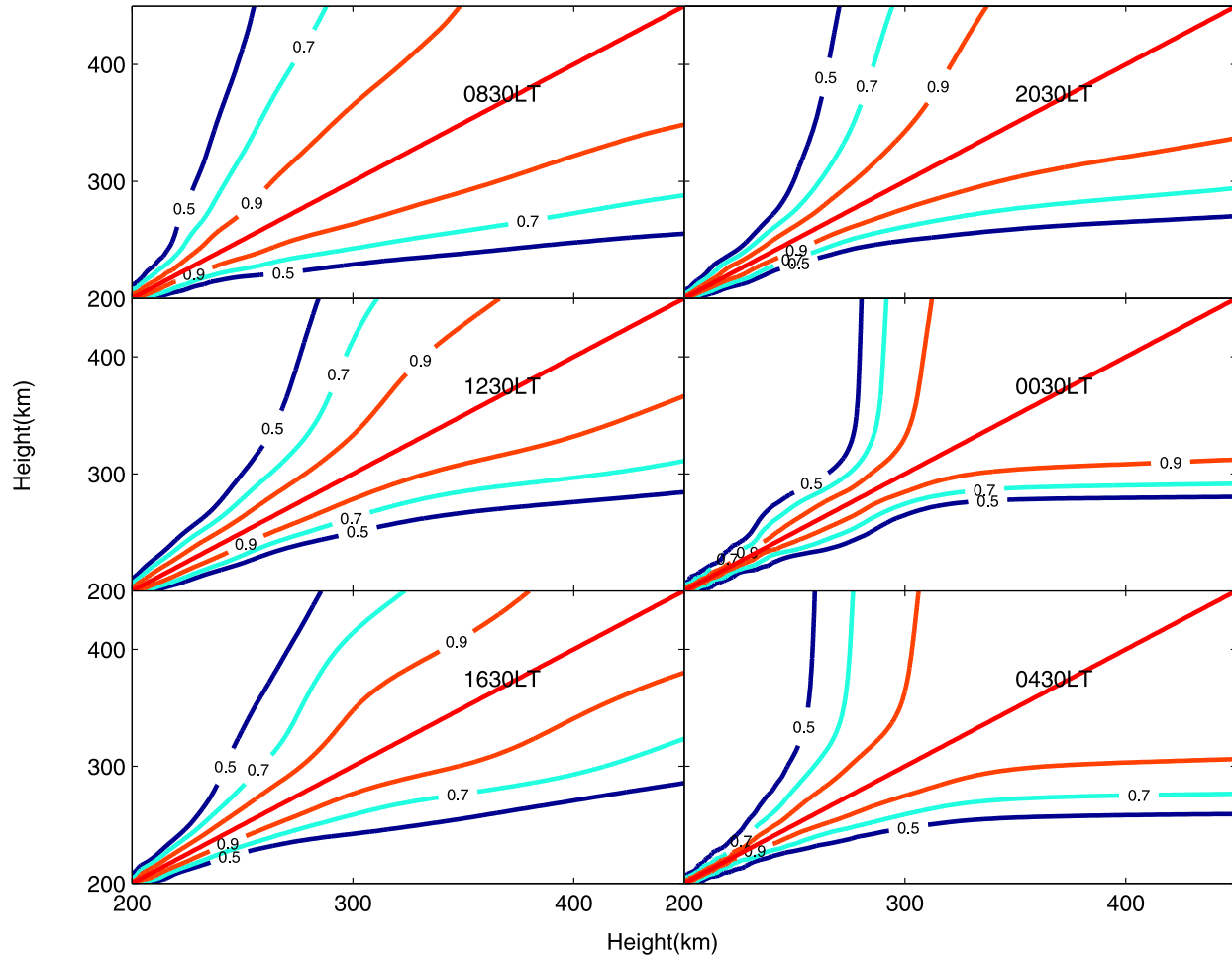


**Figure 6.** Background error correlation coefficients of electron density between 200 and 450 km for the selected six local times. The coefficients are derived from the corresponding error covariance. The coefficients matrix is a symmetrical matrix, so the values of the isolines are symmetrical with regard to the diagonal.

the observation error is proportional to the observed electron density [Angling and Cannon, 2004]. We plotted the errors against the square of electron densities for all the grid points and local times in the lower panel of Figure 5. It can be concluded that their assumption is also appropriate for the ISR observations. The best regression coefficient is 0.043 here. However, this coefficient should be studied in further investigation because of the finite samples here. There also may be other better method to represent observation error.

#### 4. Comparison of Assimilation Results Between 3DVAR and EnKF

[18] In comparison with 3DVAR, the Kalman filter can model the error covariance forward dynamically. Though

the EnKF does not transit the error covariance by the model, it can obtain the error covariance by statistics from an ensemble of model forecasts. It is very important that the statistical covariance is accurate. To test whether the advantages of the EnKF are significant in our investigation, it is necessary to compare the data assimilation results from EnKF and 3DVAR. According to equation (15), we can test these from two aspects including correlation coefficients and variances.

##### 4.1. Correlation Coefficients Comparison

[19] Figure 6 shows the correlation coefficients of electron density between 200 and 450 km (the range that the observations are assimilated) derived from the error covariance of EnKF. It can be seen that the correlation coefficients have obvious altitude and local time varia-

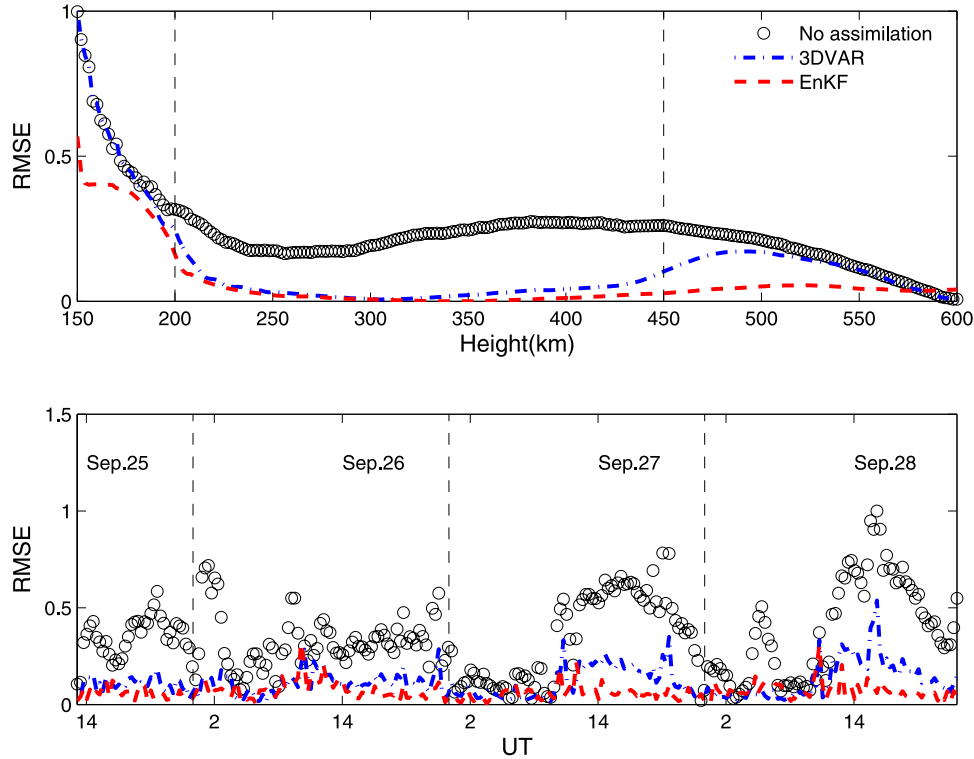


**Figure 7.** (top) Altitude and (bottom) time variations of normalized RMSE for the interval of 25–28 September 2000, between 150 and 600 km for the model results with no assimilation, 3DVAR data assimilation, and EnKF data assimilation, respectively. Two vertical lines in the top panel correspond to the upper and lower boundaries of the observations that are assimilated.

tions. With increasing altitude, the correlation coefficient between two points with the same distance will become higher for the six selected local times. Take the result of 1230 LT as an example, the correlation coefficient between 200 and 300 km is less than 0.5, while it is higher than 0.7 between 300 and 400 km. We will further discuss about the vertical correlation coefficient of the electron density in the discussion section. In comparison with 3DAVR, which assumes a static correlation coefficient here (actually time and altitude dependent correlation coefficients can also be used), the EnKF can model the altitude and local time variations of the correlation coefficients, which is more close to the real situations.

#### 4.2. Assimilation Performance Comparison

[20] To assess the performance of the data assimilation results by 3DVAR and EnKF, we calculate the Root Mean Square error (RMSE) of the relative deviation of electron density from observation, which is defined by the formula:

$$RMSE = \sqrt{\frac{1}{N} \sum_{i=1}^N \left( \frac{Ne_{mod}(i) - Ne_{obs}(i)}{Ne_{obs}(i)} \right)^2} \quad (16)$$

where  $Ne_{mod}$  and  $Ne_{obs}$  are electron density of model results and observations, respectively; and  $i$  denotes time step or the altitude.

[21] Figure 7 shows the altitude and universal time variations for the normalized RMSE of the model results with no assimilation, 3DVAR assimilation, and EnKF assimilation respectively. As expected, the RMSE of the modeled electron density by both data assimilation methods (3DVAR and EnKF) is less than that with no data assimilation in the whole space and time range (except at the upper boundary for EnKF). For 200–450 km, where the observations are assimilated, EnKF performs better than 3DVAR. This is mostly because that EnKF can get variable background error correlation coefficients versus altitude and time, which is more consistent with the real situations. While at 150–200 km and 450–600 km, where the observations are available but not assimilated into the model, EnKF also obviously perform better than 3DVAR. As illustrated above, the EnKF can model the local time and altitude variations of the correlation coefficients dynamically. It suggests that the EnKF has a better transition from data-rich regions to data-gap regions than that of 3DVAR. From the

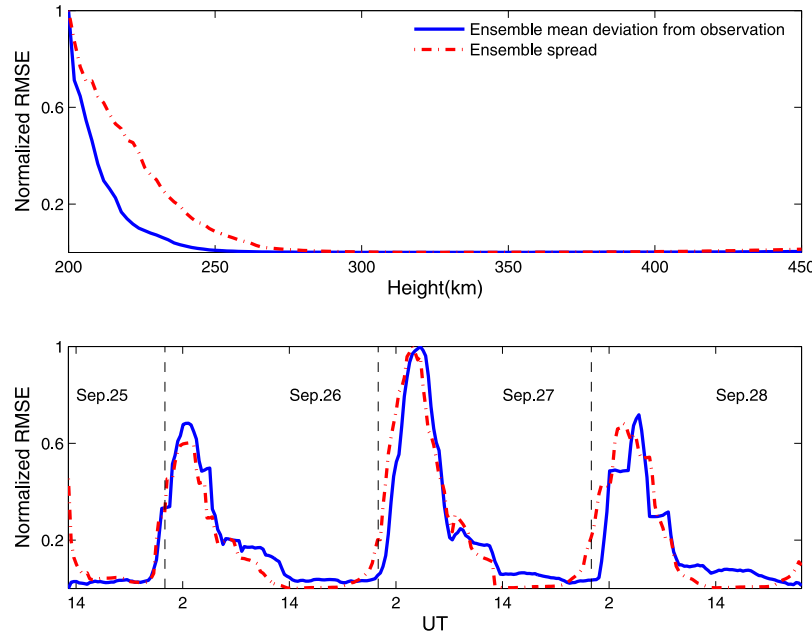


**Figure 8.** Normalized RMSE of the relative deviations of electron density for ensemble spread (dash-dotted lines) and of ensemble mean from observations (solid lines), respectively. The top and bottom panels are for the altitude (200–450 km, where observations are assimilated) variation and time step (25–28 September 2000) variation, respectively.

temporal variations of the RMSE, both data assimilation methods can obtain smaller RMSE especially during daytime, but EnKF has a better performance than 3DVAR. It should be pointed out that if accurate correlation coefficients of background error are given or the derived correlation model from observations or EnKF is used in 3DVAR, these conclusions may be different. However, accurate representation of background error correlation is usually difficult to get, while EnKF provides a probable approach. In addition, the choices of the values of several ratios in representing the observations errors, the background error covariance in 3DVAR, the perturbations of initial and boundary conditions in EnKF can also affect the above conclusions.

## 5. Assimilation Results of EnKF

[22] The prominent feature of EnKF is that the background error covariance is obtained by statistics from an ensemble of model forecasts. It is very important to assess whether the spread of the ensemble members is consistent with the deviation of ensemble mean from observations [Evensen and van Leeuwen, 1996]. Figure 8

shows the normalized RMSE of the ensemble spread and the ensemble mean as functions of altitude and time. From this figure, we can see that, both the altitude and time variations of the RMSE for the ensemble spread and ensemble mean have approximately the same shape. That is to say, the spread of the ensemble members can follow the deviations of ensemble mean from observations. It is a key factor that determines the success of the EnKF assimilation. As described above, the best estimation of the state is a weighted average of the model estimate and the observation. The weights of model state and observation are related with their error covariance closely. According to Figure 8, when the deviation of the ensemble mean from the truth state increases, the spread of the ensemble will also enlarge, and then the corresponding weight is naturally small because the corresponding background error covariance will become large.

[23] The comparison of modeled foF2 and hmF2 without or with assimilation (EnKF) and the observed values are shown in Figure 9. When without data assimilation, the modeled foF2 and hmF2 have obvious deviations from observations especially during daytime.

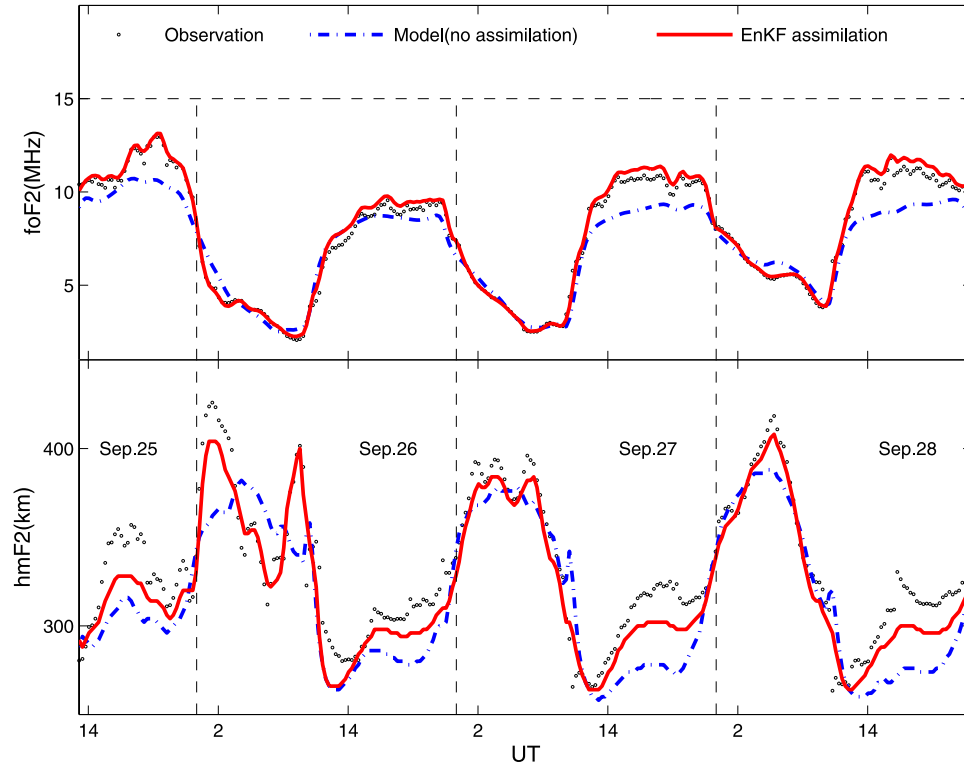


**Figure 9.** Observed (circles), modeled (with no assimilation, dash-dotted lines), and EnKF assimilated (solid lines) foF2 (top) and hmF2 (bottom) for the interval of 25–28 September 2000.

In comparison with model results without data assimilation, EnKF assimilation has a less deviation from observation for both foF2 and hmF2, especially for foF2.

## 6. Discussion

### 6.1. Vertical Correlation Coefficients of Electron Density

[24] In the 3DVAR data assimilation, an assumed background error covariance and observation error covariance are needed. The choice of error covariance will have a significant effect on the best estimation of the state since the weight of observation and background are related with corresponding error covariance. In most systems, the observation errors are assumed to be independent [Bust *et al.*, 2004]. In both 3DVAR and EnKF data assimilation performed in this paper, we also adopt the same assumption. So it is very important for us to represent the background error covariance properly. The error covariance can be decomposed to be the product of variance and correlation coefficients as shown in equation (15). The electron density errors are assumed to be proportional to the corresponding electron density and its

validation has been confirmed by statistical analysis on ISR observations in section 3.4 [Angling and Cannon, 2004; Hajj *et al.*, 2004; Mandrake *et al.*, 2005]. At last the specific representation of background error covariance is determined by a specific representation of background correlation coefficients. Essentially, the background error covariance determines the influences from data-rich regions to data-gap regions through correlation coefficients. Except for 3DVAR, there should also be an accurate representation of the initial forecast error covariance in Kalman filter [Mandrake *et al.*, 2005; Scherliess *et al.*, 2006a, 2006b].

[25] The vertical error correlation of electron densities is not well investigated yet. In the 3DVAR assimilation of this paper, the background error is considered to be Gaussian correlated with a fixed correlation length as did in Bust *et al.* [2004] in the range of 100–600 km. We also calculate the correlation coefficients at different altitudes and local times by the background error covariance derived from the ensemble. The results indicate that the correlation coefficients have obvious altitude and local time variations (Figure 6). To confirm the vertical correlation coefficients derived from the ensemble modeling results, we also calculate the correlation coeffi-

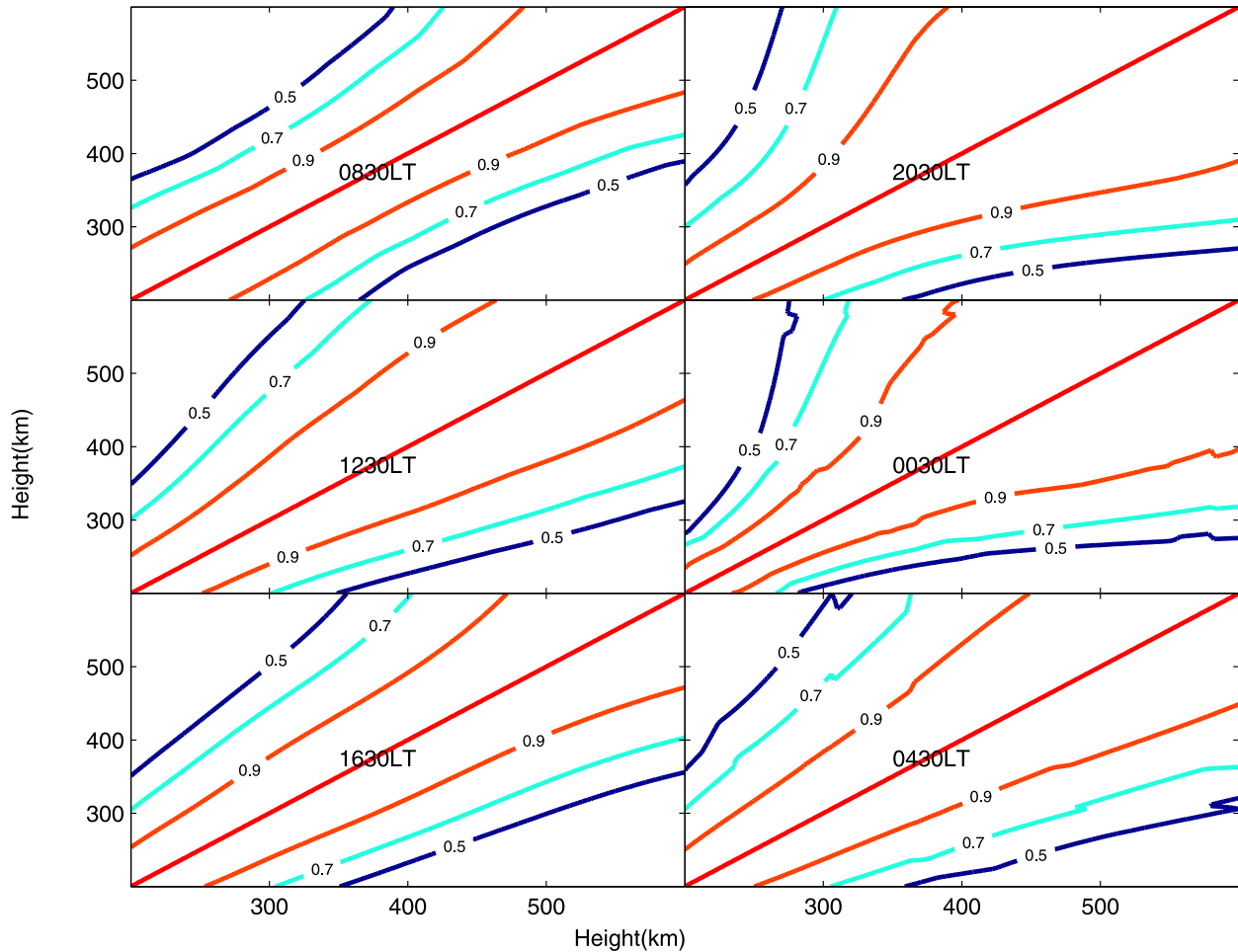


**Figure 10.** The same as Figure 6, but for results derived from observed electron density between 200 and 600 km.

coefficients from ISR observations to make a comparison. The calculation processes has been described in section 3.3. The correlation coefficients for the six same selected local times as Figure 6 are illustrated in Figure 10. It can be seen that the correlation coefficients calculated from the observed electron density profiles are consistent with the ensemble model results (Figure 6) except some minor quantitative differences at the low altitudes. This illuminates the reliability of the ensemble model results for correlation coefficients of electron density.

[26] The variations of the electron density are mainly controlled by the photo-chemical processes and dynamical processes. With the increase of altitude, the effect of the dynamical process becomes dominant. The effect of dynamics process is more important at night than by day because of the absence of solar radiation at night. These variations of control factors probably result in the altitude and local time variations of the correlation coefficients of

electron density. However, further investigations are needed to address this issue.

## 6.2. Influence of the Ensemble Size on the Assimilation

[27] In the EnKF data assimilation, the use of a finite ensemble size will introduce some errors in the estimates of the statistical moments used in the assimilation algorithm. Statistical noise in the covariance will result in incorrect relative weights between background and observation, and noise in the covariance functions will exist all through the domain and contribute to unsystematic errors in the assimilation. These errors can be decreased by increasing the ensemble size theoretically, but a very large ensemble size is not affordable in practical applications for the complicated models [Evensen and van Leeuwen, 1996; Hamill, 2004].

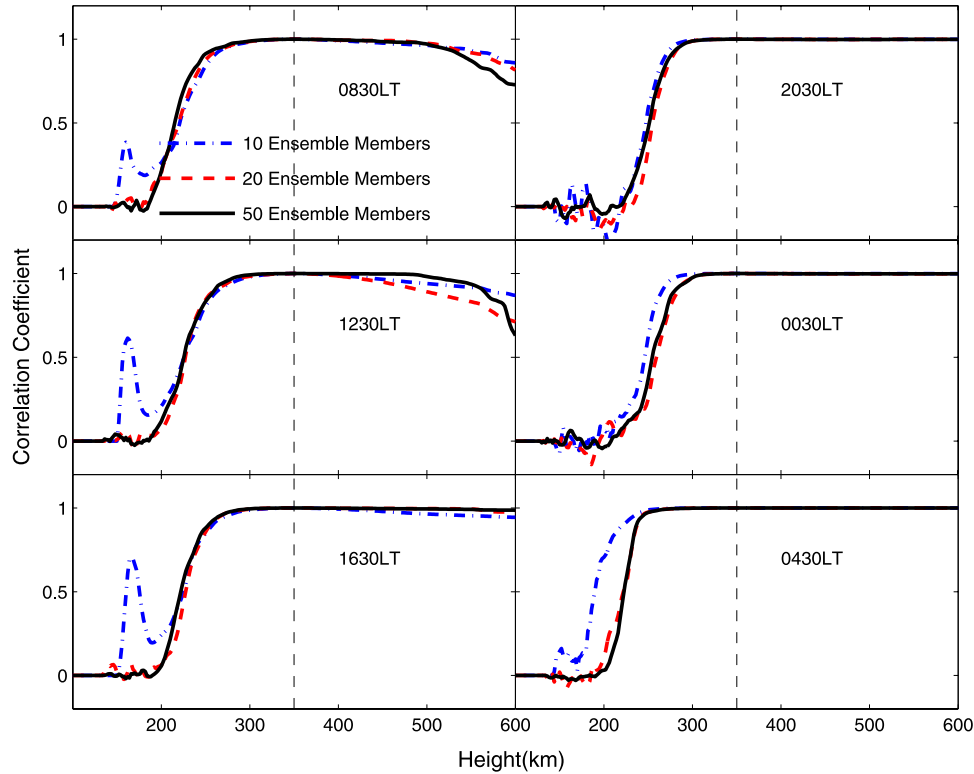


**Figure 11.** The correlation coefficients of electron density between 350 km and other heights from 100–600 km for the selected six local times. The dash-dotted lines, dashed lines, and solid lines represent the corresponding coefficients of 10, 20, and 50 ensemble members, respectively.

[28] Figure 11 shows an example of the influence of ensemble size on assimilation. The correlation coefficients between 350 km altitude and other altitudes from 100–600 km for six selected local times are illustrated in the figure. Three different ensemble sizes (10, 20, and 50) are chosen to make a comparison. According to *Houtekamer and Mitchell* [1998], there are usually many illusive strong correlations between the points which should be weakly correlated when the ensemble size is inadequate. As illustrated in the figure, the correlation coefficients with 10 ensemble members have more obvious fluctuations than that of 20 and 50 ensemble members at the altitude that weakly correlated with 350 km altitude (<200 km). The factors which may have effects on the correlations of electrons such as dynamical effect have no abrupt enhanced correlation between 350 km and the altitude <200 km, so we think that the obvious fluctuations are illusive correlations because of the relatively small number of ensemble numbers.

[29] The background error covariances are typically estimated imperfectly with a small ensemble, resulting in a bad assimilation output or even filter divergence [*Hamill*, 2004]. Though more ensemble members would

be desirable to reduce the sampling error in estimating background error covariances, it may cause more computational expense. One common algorithmic modification to improve error covariance estimates from ensembles is covariance localization [*Hamill*, 2004]. The covariance estimates from the ensemble is multiplied point by point with a correlation function that is 1 at the observation location and zero beyond some pre-specified distance. *Houtekamer and Mitchell* [1998] simply used a cut-off radius so that observations are not assimilated beyond a certain distance from the grid point. This may be problematic in situations where observations are sparse. *Houtekamer and Mitchell* [2001] put forward a preferable approach which uses a correlation function that decreases monotonically with increasing distance. In our study, we do not apply methods described above to improve error covariance estimations, since 10 ensemble members are sufficient to give a good estimation of electron density and no filter divergence occurs by our test, though there are some illusive correlations between distances that are weakly correlated. However, this problem should be carefully dealt with in practical applications as it may cause very

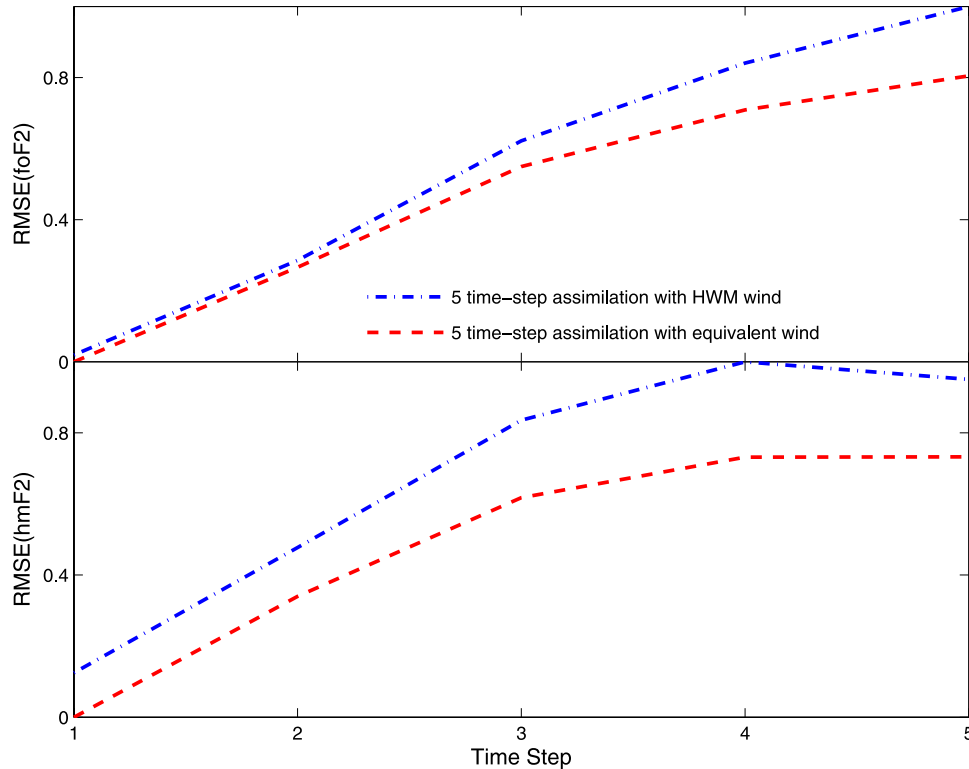


**Figure 12.** Normalized RMSE of relative deviations of (top) foF2 and (bottom) hmF2 with 5 time step assimilation from observations versus forecast time steps. Dash-dotted and dashed lines are for assimilation results with HWM wind and equivalent wind, respectively.

serious results. The problem of ensemble size and which is the most proper size number in ionospheric EnKF data assimilation need further investigations.

### 6.3. Effect of the Model Drivers

[30] Because of the lack of reliable specifications of the ionospheric driving forces, including the convection electric fields and particle precipitation at high latitudes, the low latitude electric fields, and the global neutral winds and composition, it is usually not easy to forecast the ionosphere. To achieve a better prediction performance, the external driving forces should also be adjusted simultaneously to be more close to the real weather conditions. The JPL/USC GAIM estimates the  $E \times B$  drift and/or thermospheric wind in the magnetic meridional planes simultaneously by applying the 4DVAR method with the adjoint technique [Pi *et al.*, 2003, 2004b]. The USU GAIM obtains the main ionospheric drivers by adjusting the corresponding empirical models to bring agreement between models and measurements [Schunk *et al.*, 2004].

[31] In midlatitude area, neutral composition, temperature, and wind are main driving forces. Zhang *et al.*

[1999, 2001, 2002, 2003] and Lei *et al.* [2004b, 2004c] have developed a method to derive neutral information by minimizing the difference between model results and observations by ISR or ionosonde. To improve the performance of the EnKF assimilation model, a more accurate representation of neutral composition, temperature, and wind is also very important. In the following we will test the effect of drivers on the capability of forecast.

[32] We use a simple method called equivalent wind method to adjust the neutral wind to test the feasibility of enhancing forecast capability of the EnKF assimilation model by adjusting driving forces. As we know, ionosphere peak height (hmF2) has a close relationship with the neutral meridional wind [Liu *et al.*, 2003]. The equivalent wind can be derived from the observed hmF2. In this investigation we use the method by Liu *et al.* [2003, 2004] to derive the equivalent wind. The assimilation is performed every 5 time steps. Then the equivalent winds are calculated after every assimilation step. We then calculate an increment by subtracting the meridional wind of HWM93 model at hmF2 from the derived equivalent wind. The profile of meridional wind of HWM93 model is improved by adding this increment.

In the subsequent prediction time steps, a weighted average of the improved meridional wind and of the corresponding HWM93 model results is used as input neutral meridional wind. We also run the model with 5 time step assimilation using only HWM93 model wind to make a comparison. Normalized RMSE of relative deviations of foF2 (top panel) and hmF2 (bottom panel) with 5 time step assimilation from observations are plotted versus forecast time steps in Figure 12. Dash-dotted lines and dashed lines are for assimilation results with HWM wind and equivalent wind, respectively. According to the figure, the RMSE for foF2 and hmF2 of assimilation model using equivalent wind is obviously smaller than that with no equivalent wind in both the time that assimilation is performed (time step 1) and the succedent prediction process (time step 2–5). This illustrates that the using of equivalent wind method indeed has an active effect on the prediction. Furthermore, it can only decrease the RMSE, but can not eliminate the RMSE by using equivalent wind because there are also other driving forces such as neutral composition, neutral temperature that have not been accurately represented.

## 7. Conclusions

[33] In this paper, the incoherent scatter radar (ISR) observed electron densities are assimilated into a mid-latitude ionospheric theoretical model by using an ensemble Kalman filter (EnKF) technique. To illustrate the own characteristic of EnKF method, comparisons with 3DVAR are also performed. The results can be concluded as follows:

[34] 1. In comparison with 3DVAR, the EnKF can model the correlation coefficients of electron density dynamically. Model results of the EnKF data assimilation indicate that the vertical correlation coefficients of electron density have obvious altitude and local time variations. The ISR observations also confirm these variations. The local time and altitude variations of the correlation coefficients can generally be interpreted by the corresponding variations of the control factors. However, further modeling and analysis of observations are needed to address this issue. Both the altitude and the time step variations of the ensemble spread and standard deviations of the observations have approximate the same shape, indicating that the spread of the ensemble members can follow the deviations of ensemble mean from observations and that the perturbations with normal distribution that added to the initial and boundary conditions can represent the corresponding uncertainty very well.

[35] 2. Both 3DVAR and EnKF data assimilation methods can obtain a smaller RMSE than that of model results with no assimilation. In comparison with 3DVAR,

the EnKF assimilation has a better performance with the situation of our choice of several coefficients. The EnKF has a better transition from data-rich regions to data-gap regions than that of 3DVAR, because that EnKF can model the background error covariance forward in time and model the altitude and local time variations of the correlation coefficients.

[36] 3. The external driving forces of the model also are very important for better forecast in the data assimilation. For example, the performance of prediction can be improved by adjusting neutral meridional wind using equivalent wind method.

[37] 4. In the EnKF data assimilation, there are usually many illusive correlations between the points with large distance when the ensemble size is inadequate. This problem can be avoided by using a large ensemble size.

[38] **Acknowledgments.** This work is supported by the KIP Pilot Project (kzcx2-yw-123) of CAS, National Science Foundation of China (40636032, 40725014), and National Important Basic Research Project (2006CB806306). Millstone Hill data were obtained through the Madrigal Database which is assembled and maintained by members of MIT Haystack Observatory Atmospheric Science Group. NCAR is supported by the U.S. National Science Foundation.

## References

- Anderson, D. N. (1973a), A theoretical study of the ionospheric F region equatorial anomaly, Theory, I., *Planet. Space Sci.*, *21*, 409–419.
- Anderson, D. N. (1973b), A theoretical study of the ionospheric F region equatorial anomaly, II. Results in the American and Asia sectors, *Planet. Space Sci.*, *21*, 421–442.
- Anderson, J. L., and S. L. Anderson (1998), A Monte Carlo implementation of the nonlinear filtering problem to produce ensemble assimilations and forecasts, *Mon. Weather Rev.*, *127*, 2741–2758.
- Angling, M. J., and P. S. Cannon (2004), Assimilation of radio occultation measurements into background ionospheric models, *Radio Sci.*, *39*, RS1S08, doi:10.1029/2002RS002819.
- Bailey, G. J., N. Balan, and Y. Z. Su (1997), The Sheffield University plasmasphere ionosphere model—a review, *J. Atmos. Sol. Terr. Phys.*, *59*, 1541–1552.
- Bilitza, D. (2001), International Reference Ionosphere 2000, *Radio Sci.*, *36*, 261–275.
- Bouttier, F., and P. Courtier (1999), Data assimilation concepts and methods, in *Meteorological Training Course Lecture Series*, Eur. Cent. for Medium-Range Weather Forecasts, Reading, UK.
- Bust, G. S., T. W. Garner, and T. L. Gaussiran II (2004), Ionospheric Data Assimilation Three-Dimensional (IDA3D): A global, multisensor, electron density specification algorithm, *J. Geophys. Res.*, *109*, A11312, doi:10.1029/2003JA010234.
- Codrescu, M. V., T. J. Fuller-Rowell, and C. F. Minter (2004), An ensemble-type Kalman filter for neutral thermospheric

- composition during geomagnetic storms, *Space Weather*, 2, S11002, doi:10.1029/2004SW000088.
- Daley, R. (1991), *Atmospheric Data Analysis*, 457 pp., Cambridge Univ. Press, New York.
- Eccles, J. V. (2004), Assimilation of global-scale and mesoscale electric fields from low-latitude satellites, *Radio Sci.*, 39, RS1S09, doi:10.1029/2002RS002810.
- Evensen, G. (1994), Sequential data assimilation with a nonlinear quasi-geostrophic model using Monte Carlo methods to forecast error statistics, *J. Geophys. Res.*, 99, 10,143–10,162.
- Evensen, G. (2003), The ensemble Kalman filter: theoretical formulation and practical implementation, *Ocean Dyn.*, 53, 343–367.
- Evensen, G., and P. J. van Leeuwen (1996), Assimilation of Geosat altimeter data for the Agulhas Current using the ensemble Kalman filter with a quasi-geostrophic model, *Mon. Weather Rev.*, 124, 85–96.
- Fuller-Rowell, T. J., G. H. Millward, A. D. Richmond, and M. V. Codrescu (2002), Storm-time changes in the upper atmosphere at low latitudes, *J. Atmos. Sol. Terr. Phys.*, 64, 1383–1391.
- Fuller-Rowell, T. J., C. F. Minter, and M. V. Codrescu (2004), Data assimilation for neutral thermospheric species during geomagnetic storms, *Radio Sci.*, 39, RS1S03, doi:10.1029/2002RS002835.
- Hajj, G. A., L. C. Lee, X. Pi, L. J. Romans, W. S. Schreiner, P. R. Strauss, and C. Wang (2000), COMIC GPS ionospheric sensing and space weather, *Terr. Atmos. Oceanic Sci.*, 11(1), 235–272.
- Hajj, G. A., B. D. Wilson, C. Wang, X. Pi, and I. G. Rosen (2004), Data assimilation of ground GPS total electron content into a physics-based ionospheric model by use of the Kalman filter, *Radio Sci.*, 39, RS1S05, doi:10.1029/2002RS002859.
- Hamill, T. M. (2004), Ensemble-based atmospheric data assimilation, Univ. of Colo., Boulder.
- Hedin, A. E. (1991), Extension of the MSIS thermospheric model into the middle and lower atmosphere, *J. Geophys. Res.*, 96, 1159–1172.
- Hedin, A. E., et al. (1996), Empirical wind model for the upper, middle and lower atmosphere, *J. Atmos. Sol. Terr. Phys.*, 58, 1421–1447.
- Houtekamer, P. L., and H. L. Mitchell (1998), Data assimilation using an ensemble Kalman filter technique, *Mon. Weather Rev.*, 126, 796–811.
- Houtekamer, P. L., and H. L. Mitchell (2001), A sequential ensemble Kalman filter for atmospheric data assimilation, *Mon. Weather Rev.*, 129, 123–137.
- Howe, B. M., K. Runciman, and J. A. Secan (1998), Tomography of the ionosphere: Four-dimensional simulations, *Radio Sci.*, 33(1), 109–128.
- Huba, J. D., G. Joyce, and J. A. Fedder (2000), Sami2 is another model of the ionosphere (SAMI2): A new low latitude ionospheric model, *J. Geophys. Res.*, 105(A10), 23,035–23,053.
- Kalnay, E. (2003), *Atmospheric Modeling, Data Assimilation and Predictability*, Univ. of Cambridge, UK.
- Khattatov, B., M. Murphy, M. Gnedin, B. Cruickshank, J. Adams, V. Yudin, and T. Fuller-Rowell (2004), An ionospheric forecasting system, paper presented at Institute of Navigation Annual Technical Meeting, Long Beach, Calif., Sept.
- Khattatov, B., M. Gnedin, M. Murphy, B. Cruickshank, J. Adams, V. Yudin, T. Fuller-Rowell, J. W. Wright, N. A. Zabolin, and M. J. Angling (2005), An AFRL sponsored ionospheric specification system, in *Proceedings of the 11th Ionospheric Effects Symposium*, edited by J. M. Goodman, pp. 501–511, Off. of Nav. Res., Arlington, Va.
- Lei, J. (2005), Statistical analysis and modeling investigation of midlatitude ionosphere, Ph.D. thesis, Wuhan Inst. of Phys. and Math., Chin. Acad. of Sci., Wuhan, China.
- Lei, J., L. Liu, W. Wan, and S.-R. Zhang (2004a), Model results for the ionospheric lower transition height over midlatitude, *Ann. Geophys.*, 22, 2037–2045.
- Lei, J., L. Liu, W. Wan, and S.-R. Zhang (2004b), Modeling the behavior of ionosphere above Millstone Hill during the September 21–27, 1998 storm, *J. Atmos. Sol. Terr. Phys.*, 66, 1093–1102.
- Lei, J., L. Liu, W. Wan, and S.-R. Zhang (2004c), Modeling investigation of ionospheric storm effects over Millstone Hill during August 4–5, 1992, *Earth Planets Space*, 56(9), 903–908.
- Lei, J., L. Liu, W. Wan, S.-R. Zhang, and J. M. Holt (2004d), A statistical study of ionospheric profile parameters derived from Millstone Hill incoherent scatter radar measurements, *Geophys. Res. Lett.*, 31, L14804, doi:10.1029/2004GL020578.
- Liu, L., X. Luan, W. Wan, B. Ning, and J. Lei (2003), A new approach to the derivation of dynamic information from ionosonde measurements, *Ann. Geophys.*, 21(11), 2185–2191.
- Liu, L., X. Luan, W. Wan, J. Lei, and B. Ning (2004), Solar activity variations of equivalent winds derived from global ionosonde data, *J. Geophys. Res.*, 109, A12305, doi:10.1029/2004JA010574.
- Mandrake, L., B. Wilson, C. Wang, G. Hajj, A. Mannucci, and X. Pi (2005), A performance evaluation of the operational Jet Propulsion Laboratory/University of Southern California Global Assimilation Ionospheric Model (JPL/USC GAIM), *J. Geophys. Res.*, 110, A12306, doi:10.1029/2005JA011170.
- Maybeck, P. S. (1979), *Stochastic Models, Estimation, and Control*, vol. 1, Academic, San Diego, Calif.
- Millward, G. H., R. J. Moffett, W. Quegan, and T. J. Fuller-Rowell (1996), A coupled thermospheric-ionospheric-plasmasphere Model (CTIP), in *STEP: Handbook of Ionospheric Models*, edited by R. W. Schunk, p. 173, Utah State Univ., Logan.
- Mitchell, H. L., and P. L. Houtekamer (2000), An adaptive ensemble Kalman filter, *Mon. Weather Rev.*, 128, 416–433.

- Mitchell, H. L., P. L. Houtekamer, and G. Pellerin (2002), Ensemble size, and model-error representation in an ensemble Kalman filter, *Mon. Weather Rev.*, *130*, 2791–2808.
- Pavlov, A. V., M. J. Buonsanto, A. C. Schlesier, and P. G. Richards (1999), Comparison of models and data at Millstone Hill during the 5–11 June 1991 storm, *J. Atmos. Sol. Terr. Phys.*, *61*, 263–279.
- Pi, X., C. Wang, G. A. Hajj, G. Rosen, B. D. Wilson, and G. J. Bailey (2003), Estimation of  $E \times B$  drift using a global assimilative ionospheric model: An observation system simulation experiment, *J. Geophys. Res.*, *108*(A2), 1075, doi:10.1029/2001JA009235.
- Pi, X., G. A. Hajj, B. D. Wilson, A. J. Mannucci, A. Komjathy, L. Mandrake, C. Wang, and I. G. Rosen (2004a), Three-dimensional assimilative ionospheric modeling for regions of large TEC gradient, paper presented at National Technical Meeting, Inst. of Navig., San Diego, Jan.
- Pi, X., C. Wang, G. A. Hajj, G. Rosen, B. D. Wilson, and A. J. Mannucci (2004b), Assimilative modeling of low-latitude ionosphere, paper presented at PLANS 2004, Inst. of Electr. and Electron. Eng., Monterey, Calif., 26–29 April.
- Retterer, J. M., D. T. Decker, W. S. Borer, R. E. Daniell Jr., and B. G. Fejer (2005), Assimilative modeling of the equatorial ionosphere for scintillation forecasting: Modeling with vertical drifts, *J. Geophys. Res.*, *110*, A11307, doi:10.1029/2002JA009613.
- Richards, P. G., and D. G. Torr (1985), Seasonal, diurnal, and solar cyclical variations of the limiting  $H^+$  flux in the Earth's topside ionosphere, *J. Geophys. Res.*, *90*, 5261–5268.
- Richards, P. G., J. A. Fennelly, and D. G. Torr (1994), EUVAC: a solar EUV flux model for aeronomic calculations, *J. Geophys. Res.*, *99*, 8981–8992.
- Richmond, A. D., and Y. Kamide (1988), Mapping electrodynamic features of the high-latitude ionosphere from localized observations: Technique, *J. Geophys. Res.*, *93*, 5741–5759.
- Richmond, A. D., et al. (1988), Mapping electrodynamic features of the high-latitude ionosphere from localized observations: Combined incoherent scatter radar and magnetometer measurements for January 18–19, 1984, *J. Geophys. Res.*, *93*, 5760–5776.
- Rishbeth, H., and M. Mendillo (2001), Patterns of F2-layer variability, *J. Atmos. Sol. Terr. Phys.*, *63*, 1661–1680.
- Roble, R. G., E. C. Ridley, A. D. Richmond, and R. E. Dickinson (1988), A coupled thermosphere and ionosphere general circulation model, *Geophys. Res. Lett.*, *15*, 1325–1328.
- Scherliess, L., R. W. Schunk, J. J. Sojka, and D. C. Thompson (2004), Development of a physics-based reduced state Kalman filter for the ionosphere, *Radio Sci.*, *39*, RS1S04, doi:10.1029/2002RS002797.
- Scherliess, L., R. W. Schunk, J. J. Sojka, and D. Thompson (2006a), Ionospheric/thermospheric variability at middle latitudes obtained from the full physics-based GAIM model, *Eos Trans. AGU*, *87*(52), Fall Meet. Suppl., Abstract SA12A-03.
- Scherliess, L., R. W. Schunk, J. J. Sojka, D. C. Thompson, and L. Zhu (2006b), Utah State University Global Assimilation of Ionospheric Measurements Gauss-Markov Kalman filter model of the ionosphere: Model description and validation, *J. Geophys. Res.*, *111*, A11315, doi:10.1029/2006JA011712.
- Schlüter, S., et al. (2003), Monitoring of three-dimensional ionospheric electron density distributions based on GPS measurements, in *First CHAMP Mission Results for Gravity, Magnetic and Atmospheric Studies*, edited by C. Reigber, H. Lühr, and P. Schwintzer, pp. 521–527, Springer, Berlin.
- Schunk, R. W., and A. F. Nagy (1978), Electron temperature in the F region of the ionosphere: theory and observations, *Rev. Geophys.*, *16*(3), 355–399.
- Schunk, R. W., J. J. Sojka, J. V. Eccles, and D. Thompson (1998), Expanded capabilities for the ionospheric forecast model, *AFRL Rep. AFRL-VSHATR-98-0001*, Air Force Res. Lab., Hanscom Air Force Base, Mass.
- Schunk, R. W., L. Scherliess, and J. J. Sojka (2003), Recent approaches to modeling ionospheric weather, *Adv. Space Res.*, *31*(4), 819–828.
- Schunk, R. W., et al. (2004), Global Assimilation of Ionospheric Measurements (GAIM), *Radio Sci.*, *39*, RS1S02, doi:10.1029/2002RS002794.
- Schunk, R. W., L. Scherliess, J. Sojka, D. Thompson, and L. Zhu (2005), Ionospheric Weather Forecasting on the Horizon, *Space Weather*, *3*, S08007, doi:10.1029/2004SW000138.
- Sojka, J. J., and R. W. Schunk (1985), A theoretical study of the global F region for June solstice, solar maximum, and low magnetic activity, *J. Geophys. Res.*, *90*, 5285–5298.
- Sojka, J. J., D. C. Thompson, R. W. Schunk, T. W. Bullett, and J. J. Makela (2001), Assimilation Ionospheric Model: Development and testing with Combined Ionospheric Campaign Caribbean measurements, *Radio Sci.*, *36*(2), 247–259.
- Sojka, J. J., et al. (2003), Ionospheric data assimilation: recovery of strong midlatitudinal density gradients, *J. Atmos. Sol. Terr. Phys.*, *65*, 1087–1097.
- Spencer, P. S. J., D. S. Robertson, and G. L. Mader (2004), Ionospheric data assimilation methods for geodetic applications, paper presented at PLANS 2004, Inst. of Electr. and Electron. Eng., Monterey, Calif., 26–29 April.
- Stolle, C., S. Schlüter, S. Heise, C. Jacobi, N. Jakowski, and A. Raabe (2006), A GPS based three-dimensional ionospheric imaging tool: Process and assessment, *Adv. Space Res.*, *38*(11), 2313–2317.
- Strobel, D. F., et al. (1974), The nighttime ionosphere: E region and lower F region, *J. Geophys. Res.*, *79*, 3171–3178.
- Stubbe, P. (1972), Simultaneous solution of the time dependent coupled continuity equations, heat conduction equations, and equations of motion for a system consisting of a neutral gas, an electron gas, and a four component ion gas, *J. Atmos. Sol. Terr. Phys.*, *32*, 865–903.
- Talagrand, O. (1997), Assimilation of observations, an introduction, *J. Meteorol. Soc. Jpn.*, *75*, 191–209.

- Thompson, D. C., L. Scherliess, J. J. Sojka, and R. W. Schunk (2006), The Utah State University Gauss-Markov Kalman filter of the ionosphere: The effect of slant TEC and electron density profile data on model fidelity, *J. Atmos. Sol. Terr. Phys.*, *68*, 947–958.
- Titheridge, J. E. (1996), Direct allowance for the effect of photoelectrons in ionospheric modeling, *J. Geophys. Res.*, *101*, 357–369.
- Wang, C., G. Hajj, X. Pi, I. G. Rosen, and B. Wilson (2004), Development of the Global Assimilative Ionospheric Model, *Radio Sci.*, *39*, RS1S06, doi:10.1029/2002RS002854.
- Welch, G., and G. Bishop (2004), An introduction to the Kalman filter, *TR 95-041*, Univ. of N. C., Chapel Hill.
- Zhang, S.-R., S. Fukao, and W. L. Oliver (1999), Data modeling and assimilation studies with the MU radar, *J. Atmos. Sol. Terr. Phys.*, *61*, 563–583.
- Zhang, S.-R., W. L. Oliver, S. Fukao, and S. Kawamura (2001), Extraction of solar and thermospheric information from the ionospheric electron density profile, *J. Geophys. Res.*, *106*, 12,821–12,836.
- Zhang, S.-R., W. L. Oliver, J. M. Holt, and S. Fukao (2002), Solar EUV flux, exospheric temperature and thermospheric wind inferred from incoherent scatter measurements of electron density profile at Millstone and Shigaraki, *Geophys. Res. Lett.*, *29*(9), 1358, doi:10.1029/2001GL013579.
- Zhang, S.-R., W. L. Oliver, J. M. Holt, and S. Fukao (2003), Ionospheric data assimilation: Comparison of extracted parameters using full density profiles and key parameters, *J. Geophys. Res.*, *108*(A3), 1131, doi:10.1029/2002JA009521.
- 
- J. Lei, High Altitude Observatory, National Center for Atmospheric Research, Boulder, CO 80301, USA.
- L. Liu, W. Wan, G. Xu, X. Yue, and B. Zhao, Institute of Geology and Geophysics, Chinese Academy of Sciences, 100029 Beijing, China. (wanw@mail.iggcas.ac.cn)
- S.-R. Zhang, Haystack Observatory, Massachusetts Institute of Technology, Westford, MA 01886, USA.
- F. Zheng and J. Zhu, Institute of Atmospheric Physics, Chinese Academy of Sciences, 100029 Beijing, China.